

Analytic approach to dielectric optical bent slab waveguides

K. R. HIREMATH^{1,*}, M. HAMMER¹, R. STOFFER¹, L. PRKNA² AND J. ČTYROKÝ²

¹*MESA⁺ Research Institute, University of Twente, Enschede, The Netherlands*

²*Institute of Radio Engineering and Electronics AS CR, Prague, Czech Republic*

(*author for correspondence: E-mail: k.r.hiremath@math.utwente.nl)

Abstract. A rigorous classical analytic frequency domain model of confined optical wave propagation along 2D bent slab waveguides and curved dielectric interfaces is investigated, based on a piecewise ansatz for bend mode profiles in terms of Bessel and Hankel functions. This approach provides a clear picture of the behaviour of bend modes, concerning their decay for large radial arguments or effects of varying bend radius. Fast and accurate routines are required to evaluate Bessel functions with large complex orders and large arguments. Our implementation enabled detailed studies of bent waveguide properties, including higher order bend modes and whispering gallery modes, their interference patterns, and issues related to bend mode normalization and orthogonality properties.

Key words: bent waveguides, Bessel functions, eigenmode solver, whispering gallery modes

1. Introduction

Bent dielectric waveguides play an important role in photonic integrated circuits. Accurate evaluation of mode profiles, phase propagation constants, and of optical losses associated with the leaky wave propagation is the central task for theoretical modeling of the curved structures. The present work on this – rather old – topic is motivated by the recent interest in circular optical microresonator devices as building blocks for large-scale integrated optics (Little *et al.* 1997; Bertolotti *et al.* 2004). During our participation in a related European project (NAIS 2001), we experienced that certain notions about the properties of bend modes deserved clarification. This concerns for example, the behaviour of the mode profiles for large radial coordinates, profile integrability, mode orthogonality, or a clear picture of propagation and interference of the bend modes.¹

A sound modal analysis of bent slabs becomes particularly relevant if the mode profiles are to be employed as basis fields for a description of integrated optical microresonators with circular, ring- or disk-shaped cavities. In a

¹Partly these notions originate from the use of a ray picture for the description of bent waveguides, or from approximate models in terms of “equivalent” leaky straight waveguide profiles. We will avoid these viewpoints in the present paper.

framework of coupled mode theory (Hall and Thompson 1993; Rowland and Love 1993; Klunder *et al.* 2001), an as far as possible analytic representation of the basic field profiles on a radially unbounded domain must be regarded as highly advantageous. This is provided by the approach followed in this paper. Preliminary promising studies are contained in (Hammer *et al.* 2004; Stoffer *et al.* 2004; Čtyroký *et al.* 2004); further details will be published elsewhere (see e.g. Prkna *et al.* 2004a for steps towards a 3D generalization).

Initial models of optical bent waveguides can be found in (Marcatili 1969; Marcuse 1971). Since then, various different techniques were applied to the task. By conformal mapping (Heiblum and Harris 1975; Wassmann 1999), the bent waveguide problem can be transformed into equations for a (leaky) straight waveguide. In (Bienstman *et al.* 2002) conformal mapping with perfectly matched layer (PML) boundary conditions is used to analyze bent waveguides. In a perturbational approach (Melloni *et al.* 2001) the curvature is treated as a perturbation of a straight waveguide, and the bent waveguide modes are expressed in terms of straight waveguide fields. Other techniques of a more analytical character (e.g. WKB approximations (Berglund and Gopinath 2000), a transfer matrix approach (van der Keur 1992)), or of a numerical nature (e.g. beam propagation (Rivera 1995), the method of lines (Pregla 1996), finite difference (Kim and Gopinath 1996) or finite element discretizations (Yamamoto and Koshihara 1994)) are applied as well.

The pure analytic approach for modeling of optical bent slab waveguides is quite well known (Lewin *et al.* 1977; Pennings 1990; Vassallo 1991), though apparently hardly ever evaluated rigorously. When trying to do so, a major obstacle is encountered in the form of the necessity to compute Bessel functions of large complex order and large argument; we experienced that efficient facilities for these function evaluations are not provided by the standard numerical libraries. To overcome that hindrance, most authors resorted to approximations of the problem, such that reliable results for bent slab waveguides, e.g. for the purpose of a bend mode solver benchmark, still seem to be rare.

Using the uniform asymptotic expansions of Bessel functions as provided in Abramowitz and Stegun (1964), we found that with present standard computers it is not a problem to carry out the rigorous analytic evaluation of the problem. Section 2 introduces the bend mode ansatz and outlines the analytic steps towards a solution. Remarks on bend mode normalization and on orthogonality properties of bend modes are added in Sections 2.1 and 2.2. Section 3 summarizes the results of the analytic model for a series of bend configurations, including a comparison with benchmark results where available.

The present discussion is concerned with a frequency domain model where the (real valued) frequency or vacuum wavelength is regarded as a given parameter, and where one is interested in solutions of the Maxwell equations

for wave propagation along angular segments of the curved structures, which are characterized by a complex valued propagation constants. Alternatively, one can consider time-domain resonances which are supported by full circular cavities. In that viewpoint the field solutions are characterized by an integer azimuthal index; the frequency takes the role of a complex valued eigenvalue. Any difficulties with the complex order Bessel functions are avoided in that way, and the values for frequencies and propagation constants can be largely translated between the two viewpoints (Prkna *et al.* 2004b). However, the field solutions obtained in the latter way are not directly useful for applications where one is interested in pieces of bent waveguides only. Also for a microresonator model that combines modal solutions for bent and straight waveguides by means of coupled mode theory integrals, the fixed-frequency bend mode profiles as discussed in this paper are required.

2. Bent waveguide model

Consider a bent slab waveguide with the y -axis as the axis of symmetry as shown in Fig. 1. We assume that the material properties and the fields do not vary in the y -direction. Being specified by the radially dependent refractive index $n(r)$ (here n is piecewise constant), the waveguide can be seen as a structure that is homogeneous in the angular coordinate θ . Hence one chooses an ansatz for the bend modes with pure exponential dependence on the azimuthal angle, where the angular mode number is commonly written as a product γR with a reasonably defined bend radius R , such that γ can be interpreted as a propagation constant.

In the cylindrical coordinate system (r, θ, y) , the functional form (in the usual complex notation) of the propagating electric field \mathbf{E} and the magnetic field \mathbf{H} reads

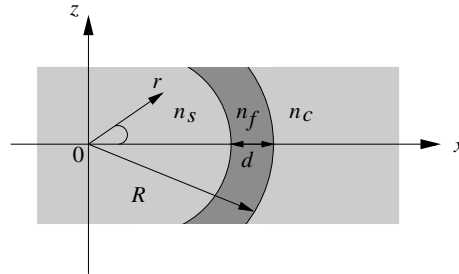


Fig. 1. A bent slab waveguide. The core of thickness d and refractive index n_f is embedded between an interior medium ('substrate') with refractive index n_s and an exterior medium ('cladding') with refractive index n_c . The distance between the origin and the outer rim of the bend defines the bend radius R .

$$\begin{aligned}\mathbf{E}(r, \theta, t) &= (\tilde{E}_r, \tilde{E}_y, \tilde{E}_\theta)(r) e^{i(\omega t - \gamma R \theta)} \\ \mathbf{H}(r, \theta, t) &= (\tilde{H}_r, \tilde{H}_y, \tilde{H}_\theta)(r) e^{i(\omega t - \gamma R \theta)}\end{aligned}\quad (1)$$

where the \sim symbol indicates the mode profile, γ is the propagation constant of the bend mode, and ω is the angular frequency corresponding to vacuum wavelength λ . Since an electromagnetic field propagating through a bent waveguide loses energy due to radiation, γ is complex valued, denoted as $\gamma = \beta - i\alpha$, where β and α are the real valued phase propagation and attenuation constants.

Note that the angular behaviour of the field (1) is determined by the product γR , where the definition of R is entirely arbitrary. Given a bend mode, the values assigned to the propagation constant γ change, if the same physical solution is described by using different definitions of the bend radius R . We will add a few more comments on this issue in Section 3.1. The definition of the bend radius R as the radial position of the outer interface of the core layer is still applicable in case the guiding is effected by a single dielectric interface only, i.e. for the description of whispering gallery modes (see Section 3.5). Hence, for this paper we stick to the definition of R as introduced in Fig. 1.

If the ansatz (1) is inserted into the Maxwell equations, one obtains the two separate sets of equations

$$\frac{\gamma R}{r} \tilde{E}_y = -\mu_0 \omega \tilde{H}_r, \quad \frac{\partial \tilde{E}_y}{\partial r} = -i\mu_0 \omega \tilde{H}_\theta, \quad \frac{1}{r} \frac{\partial r \tilde{H}_\theta}{\partial r} + \frac{i\gamma R}{r} \tilde{H}_r = -i\epsilon_0 \epsilon \omega \tilde{E}_y \quad (2)$$

and

$$\frac{\gamma R}{r} \tilde{H}_y = \epsilon_0 \epsilon \omega \tilde{E}_r, \quad \frac{\partial \tilde{H}_y}{\partial r} = i\epsilon_0 \epsilon \omega \tilde{E}_\theta, \quad \frac{1}{r} \frac{\partial r \tilde{E}_\theta}{\partial r} + \frac{i\gamma R}{r} \tilde{E}_r = i\mu_0 \omega \tilde{H}_y \quad (3)$$

with vacuum permittivity ϵ_0 , vacuum permeability μ_0 , and the relative permittivity $\epsilon = n^2$.

For transverse electric (TE) waves the only nonzero components are \tilde{E}_y , \tilde{H}_r and \tilde{H}_θ , which are expressed in terms of \tilde{E}_y , while for transverse magnetic (TM) waves the only nonzero components are \tilde{H}_y , \tilde{E}_r and \tilde{E}_θ , which are given by \tilde{H}_y . Within radial intervals with constant refractive index n , the basic electric and magnetic components are governed by a Bessel equation with complex order γR ,

$$\frac{\partial^2 \phi}{\partial r^2} + \frac{1}{r} \frac{\partial \phi}{\partial r} + (n^2 k^2 - \frac{\gamma^2 R^2}{r^2}) \phi = 0 \quad (4)$$

for $\phi = \tilde{E}_y$ or $\phi = \tilde{H}_y$, where $k = 2\pi/\lambda$ is the (given, real) vacuum wave-number. For TE modes, the interface conditions require continuity of \tilde{E}_y and of $\partial_r \tilde{E}_y$ across the dielectric interfaces. For TM modes, continuity of \tilde{H}_y and of $\epsilon^{-1} \partial_r \tilde{H}_y$ across the interfaces is required.

Equation (4), together with the interface conditions and suitable boundary conditions for $r \rightarrow 0$ and $r \rightarrow \infty$, represents an eigenvalue problem with the bend mode profiles ϕ as eigenfunctions, and the propagation constants γ or angular mode numbers $v = \gamma R$ as eigenvalues. The equation is solved piecewise in the regions with constant refractive index. While the procedure is in principle applicable for arbitrary multilayer bent waveguides, for the sake of brevity we discuss here the three layer configuration as introduced in Fig. 1.

The general solution of Equation (4) is a linear combination of the Bessel functions of the first kind J and of the second kind Y . This representation is applicable to the core region. Since Y tends to $-\infty$ if $r \rightarrow 0$, for the boundedness of the electric/magnetic field at the origin one selects only the Bessel function of the first kind J for the interior region. In the outer region, we are looking for a complex superposition of J and Y that represents outgoing waves. Such a solution can be given in terms of the Hankel functions of the first kind $H^{(1)}$ or of the second kind $H^{(2)}$. Using the asymptotic expansions of these functions (Abramowitz and Stegun, 1964, Chap. 9, Equation (9.2.3) and (9.2.4))

$$\begin{aligned} H_v^{(1)}(nkr) &\sim \sqrt{\frac{1}{\pi nkr}} e^{i(nkr - v\pi/2 - \pi/4)} \\ H_v^{(2)}(nkr) &\sim \sqrt{\frac{1}{\pi nkr}} e^{-i(nkr - v\pi/2 - \pi/4)} \end{aligned} \quad (5)$$

and taking into account the harmonic time dependence $\exp(i\omega t)$ (with positive frequency), one observes that $H^{(1)}$ represents incoming waves, while outgoing waves are given by $H^{(2)}$. Thus the piecewise ansatz for the basic components of the electric/magnetic bent mode profile is

$$\phi(r) = \begin{cases} A_s J_v(n_s kr) & \text{if } 0 \leq r \leq R^-, \\ A_f J_v(n_f kr) + B_f Y_v(n_f kr), & \text{if } R^- \leq r \leq R^+, \\ A_c H_v^{(2)}(n_c kr) & \text{for } r \geq R^+, \end{cases} \quad (6)$$

where $R^- = R - d$, $R^+ = R$, and where A_s , A_f , B_f and A_c are so far unknown constants.

The polarization dependent interface conditions lead to a homogeneous system of linear equations for A_s , A_f , B_f and A_c . The condition for a nontrivial solution can be given the form

$$\begin{aligned}
& \frac{(J_v(n_f k R^-)/J_v(n_s k R^-)) - q_s(J'_v(n_f k R^-)/J'_v(n_s k R^-))}{(Y_v(n_f k R^-)/J_v(n_s k R^-)) - q_s(Y'_v(n_f k R^-)/J'_v(n_s k R^-))} \\
&= \frac{(J_v(n_f k R^+)/H_v^{(2)}(n_c k R^+)) - q_c(J'_v(n_f k R^+)/H_v^{(2)'}(n_c k R^+))}{(Y_v(n_f k R^+)/H_v^{(2)}(n_c k R^+)) - q_c(Y'_v(n_f k R^+)/H_v^{(2)'}(n_c k R^+))} \quad (7)
\end{aligned}$$

with $q_j = n_f/n_j$ for TE polarization, and with $q_j = n_j/n_f$ for TM polarized fields, for $j = s, c$. Equation (7) is the dispersion equation for the three layer bent slab waveguide. For given frequency ω , this equation is to be solved² for the propagation constants $\gamma = v/R$.

For the numerical implementation, Equation (7) is rearranged as

$$T_1 \cdot T_2 = T_3 \cdot T_4, \quad (8)$$

where

$$\begin{aligned}
T_1 &= J_v(n_f k R^-)J'_v(n_s k R^-) - q_s J_v(n_s k R^-)J'_v(n_f k R^-), \\
T_2 &= Y_v(n_f k R^+)H_v^{(2)'}(n_c k R^+) - q_c H_v^{(2)}(n_c k R^+)Y'_v(n_f k R^+), \\
T_3 &= Y_v(n_f k R^-)J'_v(n_s k R^-) - q_s J_v(n_s k R^-)Y'_v(n_f k R^-), \\
T_4 &= J_v(n_f k R^+)H_v^{(2)'}(n_c k R^+) - q_c H_v^{(2)}(n_c k R^+)J'_v(n_f k R^+).
\end{aligned}$$

In contrast to common notions about leaky modes, the fields obtained by the ansatz (6) do not diverge for large radial coordinate r . The asymptotic expansion (5) predicts a decay $\sim 1/\sqrt{r}$. No difficulties related to ‘large’ terms are to be expected for the numerical evaluation of Equation (8). Moreover, as shown below, with the squared mode profile being accompanied by a factor r^{-1} in the relevant expression, the bend modes can even be normalized with respect to the azimuthal mode power.

2.1. BEND MODE NORMALIZATION

The power flow density associated with a bend mode is given by the time averaged Poynting vector $\mathbf{S}_{av} = \frac{1}{2} \Re(\mathbf{E} \times \mathbf{H}^*)$. The axial component $S_{av,y}$ vanishes in the 2D setting; for TE waves the radial and azimuthal components evaluate to

²In an alternative approach where one looks at time domain resonances of circular cavities, a similar procedure as outlined here (Rowland and Love 1993; Prkna *et al.* 2004b) leads to precisely the same equation (cf. the remarks in the introduction). In that case Equation (7) is to be solved for complex valued resonance frequencies ω , for given integer azimuthal mode numbers v .

$$S_{\text{av},r} = \frac{-1}{2\mu_0\omega} \Re \left[i\tilde{E}_y \frac{\partial \tilde{E}_y^*}{\partial r} \right] e^{-2\alpha R\theta}, \quad S_{\text{av},\theta} = \frac{\beta}{2\mu_0\omega} \frac{R}{r} |\tilde{E}_y|^2 e^{-2\alpha R\theta}, \quad (9)$$

and for TM polarization one obtains

$$S_{\text{av},r} = \frac{1}{2\epsilon_0\epsilon\omega} \Re \left[\tilde{H}_y^* \frac{\partial \tilde{H}_y}{\partial r} \right] e^{-2\alpha R\theta}, \quad S_{\text{av},\theta} = \frac{\beta}{2\epsilon_0\epsilon\omega} \frac{R}{r} |\tilde{H}_y|^2 e^{-2\alpha R\theta}. \quad (10)$$

The total optical power transported by the mode in the angular direction is given by $P_\theta(\theta) = \int_0^\infty S_{\text{av},\theta} dr$. Somewhat surprisingly, this expression can be considerably simplified by using the following formula (Luke, 1962, Section 11.2, Equation (5)),

$$\begin{aligned} & \int C_\mu(kx) D_\nu(kx) \frac{dx}{x} \\ &= \frac{kx}{\mu^2 - \nu^2} \{ C_\mu(kx) D_{\nu+1}(kx) - C_{\mu+1}(kx) D_\nu(kx) \} + \frac{C_\mu(kx) D_\nu(kx)}{\mu + \nu}, \end{aligned} \quad (11)$$

where C_μ , D_ν are any cylindrical functions (i.e. functions which are linear combinations of J_μ and Y_μ , or of J_ν and Y_ν , respectively). Observing that for a valid mode profile the pieces of the ansatz (6) satisfy the polarization dependent continuity conditions at the dielectric interfaces, application of Equation (11) and of several standard identities for Bessel functions leads to exact cancellation of the boundary terms that arise in the piecewise integration, with the exception of the limit term for $r \rightarrow \infty$. In that regime the mode profile is represented by the asymptotic form (5) of the relevant Hankel functions, such that one arrives at the two expressions

$$\begin{aligned} P_\theta(\theta) &= \frac{|A_c|^2}{2\mu_0\omega\alpha R\pi} e^{\alpha R(\pi-2\theta)} (\text{TE}), \\ P_\theta(\theta) &= \frac{|A_c|^2}{2\epsilon_0 n_c^2 \omega \alpha R \pi} e^{\alpha R(\pi-2\theta)} (\text{TM}) \end{aligned} \quad (12)$$

for the modal power of TE and TM polarized modes, respectively. All mode profiles shown in Section 3 are power normalized with respect to these expressions (evaluated at $\theta = 0$).

Alternatively, Equation (12) can be derived in a way quite analogous to what follows in Section 2.2: Upon integrating the vanishing divergence of

the Poynting vector $\nabla \cdot (\mathbf{E} \times \mathbf{H}^* + \mathbf{E}^* \times \mathbf{H}) = 0$ for a modal solution (\mathbf{E}, \mathbf{H}) over a differential angular segment in the domain of polar coordinates, by means of Gauss' theorem one relates the angular decay of modal power to the outflow of optical power in the radial direction. The limit of that flow for large radial coordinates exists and can be evaluated by again using the asymptotic form (5) of the mode profile, leading to expressions (12) for the modal power.

By considering the above expressions for large bend radii, one might wonder whether these may lead to a scheme for the normalization of non-guided modal solutions associated with straight waveguides as given in (Benech *et al.* 1992) in terms of plane wave superpositions. Examination of Equation (12) with the help of Equation (26), however shows that the expression (12) for the modal power is not applicable in the limit $R \rightarrow \infty$. Hence in this respect, there is no direct correspondence between the present bend modes supported by structures with low curvature and radiative modes of similar straight waveguides.

2.2. ORTHOGONALITY OF BEND MODES

If the bend mode profiles are employed as basis elements for an expansion of a general optical field in the bend structure, the orthogonality properties of these modes become relevant: Projecting on the basis modes allows to relate the modal amplitudes to the given arbitrary field. As a consequence of the leaky nature of the complex bend modes, the orthogonality relations involve nonconjugate versions of the field profiles.³

Let $(\mathbf{E}_p, \mathbf{H}_p)$ and $(\mathbf{E}_q, \mathbf{H}_q)$ be the electromagnetic fields (1) of bend modes with propagation constants γ_p and γ_q , respectively, which are supported by the same bent waveguide. We start with the identity

$$\nabla \cdot (\mathbf{E}_p \times \mathbf{H}_q - \mathbf{E}_q \times \mathbf{H}_p) = 0, \quad (13)$$

which is a straightforward consequence of the Maxwell equations.

Consider the integral of Equation (13) over an angular segment $\Omega = [0, \tilde{r}] \times [\theta, \theta + \Delta\theta]$ in the waveguide plane, specified by intervals of the polar coordinates:

$$\int_{\Omega} \nabla \cdot \mathbf{A} \, dS = 0 \quad \text{with} \quad \mathbf{A} = (A_r, A_y, A_\theta) = \mathbf{E}_p \times \mathbf{H}_q - \mathbf{E}_q \times \mathbf{H}_p. \quad (14)$$

³An approximate orthogonality relation involving complex conjugates of one of the mode profiles is derived in Morita and Yamada (1990), valid in the limit of large bend radius (i.e. for almost straight waveguides).

After simplification of Equation (14) by means of the Gauss theorem and a Taylor series expansion around θ , for small, nonzero $\Delta\theta$ one obtains

$$i(\gamma_p + \gamma_q)R \int_0^{\tilde{r}} A_\theta(r, \theta) dr = \tilde{r}A_r(\tilde{r}, \theta). \quad (15)$$

In order to evaluate the limit $\tilde{r} \rightarrow \infty$ of the right hand side, rA_r is expressed in terms of the basic mode profile components E_y and H_y , with the help of Equations (2) and (3):

$$rA_r = \frac{i}{\mu_0\omega} r(E_{p,y}\partial_r E_{q,y} - E_{q,y}\partial_r E_{p,y}) + \frac{i}{\epsilon_0\epsilon_c\omega} r(H_{p,y}\partial_r H_{q,y} - H_{q,y}\partial_r H_{p,y}). \quad (16)$$

Here $\epsilon_c = n_c^2$ is the permittivity in the exterior region of the bend (constant for large radii). In this region, the basic components $\phi_p = \tilde{E}_{p,y}$ or $\phi_p = \tilde{H}_{p,y}$ of modal solutions (6) are given by Hankel functions of second kind i.e. $\phi_p(r) = A_{c,p}H_{\gamma_p R}^{(2)}(n_c k r)$, which, for large radial coordinate, assume the asymptotic forms

$$\begin{aligned} \phi_p(r) &\sim A_{c,p} \sqrt{\frac{2}{\pi n_c k r}} e^{-i(n_c k r - \gamma_p R \pi/2 - \pi/4)}, \\ \partial_r \phi_p(r) &\sim \left(-\frac{1}{2r} - i n_c k\right) \phi_p(r). \end{aligned} \quad (17)$$

By using these expressions, the limits $r \rightarrow \infty$ of the individual parts of Equation (16) can be shown to vanish

$$\lim_{r \rightarrow \infty} [r(\phi_p \partial_r \phi_q - \phi_q \partial_r \phi_p)] = 0. \quad (18)$$

This leads to the identity

$$(\gamma_p + \gamma_q) \int_0^\infty \mathbf{a}_\theta \cdot (\mathbf{E}_p \times \mathbf{H}_q - \mathbf{E}_q \times \mathbf{H}_p) dr = 0, \quad (19)$$

where \mathbf{a}_θ is the unit vector in the azimuthal (θ -) direction.

After inspecting Equations (2) and (3), one readily sees that the fields $(\mathbf{E}_{\tilde{p}}, \mathbf{H}_{\tilde{p}})$ and the propagation constant $\gamma_{\tilde{p}}$ with

$$\begin{aligned}
\gamma_{\tilde{p}} &= -\gamma_p, \\
E_{\tilde{p},r} &= E_{p,r}, & E_{\tilde{p},y} &= E_{p,y}, & E_{\tilde{p},\theta} &= -E_{p,\theta}, \\
H_{\tilde{p},r} &= -H_{p,r}, & H_{\tilde{p},y} &= -H_{p,y}, & H_{\tilde{p},\theta} &= H_{p,\theta}
\end{aligned} \tag{20}$$

describe a valid modal solution of the bend problem. By writing out the expression (19) for the quantities with indices \tilde{p} and q , by applying the transformation (20), and by observing that $\mathbf{a}_\theta \cdot (\mathbf{E}_{\tilde{p}} \times \mathbf{H}_q - \mathbf{E}_q \times \mathbf{H}_{\tilde{p}}) = \mathbf{a}_\theta \cdot (\mathbf{E}_p \times \mathbf{H}_q + \mathbf{E}_q \times \mathbf{H}_p)$, Equation (19) can be given the form

$$(\gamma_p - \gamma_q) \int_0^\infty \mathbf{a}_\theta \cdot (\mathbf{E}_p \times \mathbf{H}_q + \mathbf{E}_q \times \mathbf{H}_p) dr = 0. \tag{21}$$

Motivated by the result (21), we define the following symmetric, complex valued inner product⁴ of two (integrable) electromagnetic fields $(\mathbf{E}_1, \mathbf{H}_1)$ and $(\mathbf{E}_2, \mathbf{H}_2)$, given in the polar coordinate system of the bend structure:

$$\begin{aligned}
(\mathbf{E}_1, \mathbf{H}_1; \mathbf{E}_2, \mathbf{H}_2) &= \int_0^\infty \mathbf{a}_\theta \cdot (\mathbf{E}_1 \times \mathbf{H}_2 + \mathbf{E}_2 \times \mathbf{H}_1) dr \\
&= \int_0^\infty (E_{1,r}H_{2,y} - E_{1,y}H_{2,r} + E_{2,r}H_{1,y} - E_{2,y}H_{1,r}) dr.
\end{aligned} \tag{22}$$

Obviously, the integrand vanishes if fields of different (2D) polarizations are inserted, i.e. TE and TM bend modes are orthogonal with respect to (22). One easily checks that the product is also zero, if the forward and backward versions (two fields with their components related by the transformation (20)) of a bend mode are inserted. Finally, according to Equation (21), two non-degenerate bend modes with propagation constants $\gamma_p \neq \gamma_q$ that are supported by the same bend structure are orthogonal with respect to the product (22). These formal statements hold for pairs of the fields (1) with the full space and time dependence, for the expressions excluding the time dependence, as well as for pairs of pure mode profiles that depend on the radial coordinate only.

Assuming that for a given bend configuration a discrete, indexed set of nondegenerate modal fields $(\mathbf{E}_p, \mathbf{H}_p)$ with (pairwise different) propagation constants γ_p is considered, the orthogonality properties can be stated in the more compact form

$$(\mathbf{E}_p, \mathbf{H}_p; \mathbf{E}_q, \mathbf{H}_q) = \delta_{p,q} N_p \tag{23}$$

⁴cf. the standard variants of orthogonality relations for straight dielectric waveguides made of attenuating materials, as introduced, for example, in Vassallo (1991).

with

$$N_p = 2 \int_0^\infty \mathbf{a}_\theta \cdot (\mathbf{E}_p \times \mathbf{H}_p) \, dr = 2 \int_0^\infty (E_{p,r} H_{p,y} - E_{p,y} H_{p,r}) \, dr, \quad (24)$$

and $\delta_{p,q} = 0$ for $p \neq q$, $\delta_{p,p} = 1$. For mode sets of uniform polarization and uniform direction of propagation, it can be convenient to write the orthogonality properties in terms of the basic mode profile components $\phi = \tilde{E}_y$ (TE) or $\phi = \tilde{H}_y$ (TM). This leads to the relations

$$\int_0^\infty \zeta \frac{\phi_p \phi_q}{r} \, dr = \delta_{p,q} P_p \quad \text{with} \quad P_p = \int_0^\infty \zeta \frac{\phi_p^2}{r} \, dr, \quad (25)$$

$\zeta = 1$ for TE, and $\zeta = 1/\epsilon(r)$ for TM polarization, which differ from the corresponding familiar expressions for straight dielectric slab waveguides by the appearance of the inverse radial coordinate r only. According to Equation (17), P_p is obviously bounded. Note, however, that here N_p and P_p are complex valued quantities.

An alternative derivation of Equation (25) starts with the eigenvalue equation (4), written out for two different modal solutions. Each equation is multiplied by the other mode profile, one subtracts the results, and integrates over the radial axis. This leads to an equation with the difference of the squared propagation constants times the integral of Equation (25) on one side, and with a limit as in Equation (16) on the other. Then the reasoning of Equations (17) and (18) can be applied to obtain the desired result. All sets of bend mode profiles shown in the following sections satisfy the relations (23) or (25), respectively, up to the accuracy that can be expected from the computational procedures.

3. Examples

The solution of Equation (7) requires the evaluation of Bessel and Hankel functions of complex order, where typically values of $v = \gamma R$ in intervals $\Re(v) \in [10^1, 10^4]$ and $\Im(v) \in [-10^{-12}, -10^{-1}]$ and arguments nkr up to 10^5 are encountered. The relevant Bessel functions are well behaved for the above values of order and argument; in particular, no terms with numerically harmful growth appear. We found that subroutines for complex order Bessel functions are not included in standard numerical libraries, therefore we had to resort to own implementations.

The procedures are based on ‘uniform asymptotic expansions’ of Bessel functions and their derivatives in terms of Airy functions (Abramowitz and Stegun 1964; Temme 1997). More specifically, Equation (9.3.35), (9.3.36), (9.3.43), and (9.3.44) from Abramowitz and Stegun (1964) were encoded, restricted to the first two terms of the summations, which we observed to be sufficient for the present examples. Routines for Airy functions with complex arguments according to Amos (1983) were adopted. Further details can be found in Hiremath (2003) and Prkna (2004).

The expansions are not applicable in a regime where the order is close to the argument of the cylindrical functions. Fortunately we are interested here in configurations that involve complex orders (γR) with negative imaginary parts ($-\alpha$), and real arguments (nkr). While cases with approximate equality of order and argument could in principle occur for bend modes with extremely low loss, for the evaluation of propagation constants and the profile plots of the examples below this transition region appeared not to be relevant. Otherwise, supplementary routines (see e.g., Temme 1997) would have to be incorporated which cover that region of parameters.

Two techniques were implemented to find the roots v of Equation (7) in the complex plane. As a heuristic search procedure, a suitably selected region of the complex plane is divided into a number of rectangles, the lower left and upper right corner points of which are then supplied as initial guesses to a root finding routine based on the secant method. Repeated roots are rejected, the remaining unique roots are sorted in descending order of their imaginary part $-\alpha$. By refining the subdivision into rectangles, it can be ascertained with reasonable robustness that all the roots in the given region are captured.

Alternatively, a root tracking procedure is implemented to solve the dispersion equation. Starting with the propagation constants of straight waveguides with a refractive index profile cross section equal to that of the given bent waveguide, a series of bends with decreasing radius are considered, with the roots found for each configuration used as initial guesses for the subsequent one. In this way, the bend propagation constants are followed in the complex plane.

Modes of different orders are indexed by counting the local minima in the absolute value of the principal electric (TE) or magnetic (TM) component of the mode profile.

Table 1. TE₀ angular mode numbers v for bent waveguides of different bend radius R according to Fig. 1, with $(n_s, n_f, n_c) = (1.6, 1.7, 1.6)$, $d = 1 \mu\text{m}$, for a vacuum wavelength $\lambda = 1.3 \mu\text{m}$

$R (\mu\text{m})$	$v = \gamma' R$, Vassallo (1991)	$v = \gamma R$, present
50.5	$4.0189 \times 10^2 - i 7.9990 \times 10^{-2}$	$4.0189 \times 10^2 - i 7.9973 \times 10^{-2}$
100.5	$8.0278 \times 10^2 - i 1.2856 \times 10^{-2}$	$8.0278 \times 10^2 - i 9.6032 \times 10^{-4}$
150.5	$1.2039 \times 10^3 - i 7.3948 \times 10^{-6}$	$1.2039 \times 10^3 - i 7.3914 \times 10^{-6}$
200.5	$1.6051 \times 10^3 - i 4.9106 \times 10^{-8}$	$1.6051 \times 10^3 - i 4.8976 \times 10^{-8}$

Table 2. TE_0 angular mode numbers v for low contrast bends according to Fig. 1, with different bend radius R and parameters $(n_s, n_f, n_c) = (3.22, 3.26106, 3.22)$, $d = 1 \mu\text{m}$, for a vacuum wavelength $\lambda = 1.3 \mu\text{m}$

$R (\mu\text{m})$	$v = \gamma' R'$, Vassallo (1991)	$v = \gamma R$, present
200.5	$3.1364 \times 10^3 - i 6.2059 \times 10^{-1}$	$3.1364 \times 10^3 - i 6.2135 \times 10^{-1}$
400.5	$6.2700 \times 10^3 - i 4.9106 \times 10^{-2}$	$6.2700 \times 10^3 - i 4.9159 \times 10^{-2}$
600.5	$9.4041 \times 10^3 - i 2.5635 \times 10^{-3}$	$9.4041 \times 10^3 - i 2.5635 \times 10^{-3}$
800.5	$1.2538 \times 10^4 - i 1.1174 \times 10^{-4}$	$1.2538 \times 10^4 - i 1.1174 \times 10^{-4}$
1000.5	$1.5673 \times 10^4 - i 4.4804 \times 10^{-6}$	$1.5673 \times 10^4 - i 4.4804 \times 10^{-5}$

3.1. PROPAGATION CONSTANTS

For purposes of validating our implementation we start with a comparison of phase propagation constants and attenuation levels. Tables 1 and 2 list values for angular mode numbers obtained with the present mode solver for two bend configurations adopted from Vassallo (1991), together with reference data from that source. We found an excellent overall agreement, for both the configurations with higher (Table 1) and lower refractive index contrast (Table 2).

The discussion of bent waveguides in Vassallo (1991) applies an alternative definition of the bend radius R' as the distance from the origin to the center of the core layer, which is related to the radius R as introduced in Fig. 1 by $R' = R - d/2$ (hence the unusual values of bend radii in Tables 1 and 2). Both definitions are meant as descriptions of the same physical configuration, i.e. both lead to the same angular field dependence (1), given in terms of the azimuthal mode numbers v as determined by the dispersion equation (7). Via the relation $v = \gamma R = \gamma' R'$, the different choices of the bend radius result in different values γ and $\gamma' = \gamma R / (R - d/2)$ for the propagation constant, and consequently in different values β , β' and α , α' for the phase and attenuation constants.

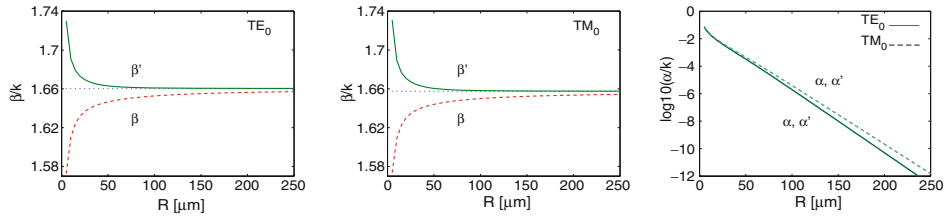


Fig. 2. Phase constants β , β' and attenuation constants α , α' versus the bend radius R , for bends according to Table 1. The dashed quantities $\beta' = \beta R / R'$ and $\alpha' = \alpha R / R'$ correspond to a description of the bend in terms of an alternative bend radius $R' = R - d/2$. The dotted lines in the first two plots indicate the levels of the effective indices of a straight waveguide with the cross section and refractive index profile of the bent slabs.

Still, for many applications one is interested in the variation of the phase constant and the attenuation with the curvature of the bend, expressed by the bend radius. Fig. 2 shows corresponding plots for the configuration of Table 1, including values for the two different bend radius definitions. While on the scale of the figure the differences are not visible for the attenuation constants, the levels of the phase propagation constants differ indeed substantially for smaller bend radii. As expected, for low curvature the values of both β/k and β'/k tend to the effective indices of straight slab waveguides with equivalent refractive index profile. For the present low contrast configuration, only minor differences between TE and TM polarization occur.

Certainly no physical reasoning should rely on the entirely arbitrary definition of the bend radius. This concerns, for example, statements about the growth or decay of phase propagation constants with R (according to Fig. 2 the sign of the slope can indeed differ), or discussions about the ‘phase matching’ of bent waveguides and straight channels in coupler or microresonator configurations. Care must be taken that values for β and α or effective quantities like β/k are used with the proper definition of R taken into account.

With the present analytic (or semi-analytic) solutions at hand, we have now a possibility to validate ‘classical’ expressions for the variation of the bend attenuation with the bend radius. Beyond the high curvature region, Fig. 2 shows a strict exponential decay of α with respect to R , as predicted by an approximate loss formula for symmetric bent slabs given in Marcuse (1972, Equations (9.6)–(24)):

$$\alpha = \frac{R - w}{R} \frac{g^2}{2\beta_s(1 + gw)} \frac{h^2}{(n_f^2 - n_s^2)k^2} \times e^{2gw} e^{-2(\beta_s \tanh^{-1}(g/\beta_s) - g)(R - w)}. \quad (26)$$

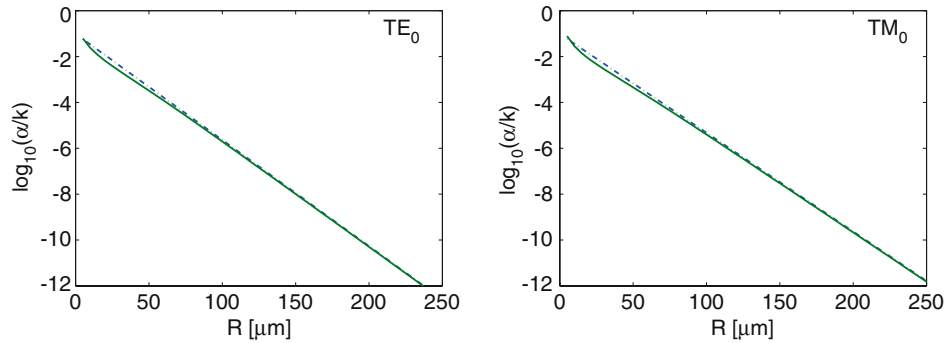


Fig. 3. Attenuation constants of the principal TE and TM modes for symmetric bent waveguides with $n_f = 1.7$, $n_s = n_c = 1.6$, $d = 1 \mu\text{m}$, $\lambda = 1.3 \mu\text{m}$, for varying bend radius R . The dashed lines show the exponential decay according to Equation (26); the solid curves are the present analytic mode solver results.

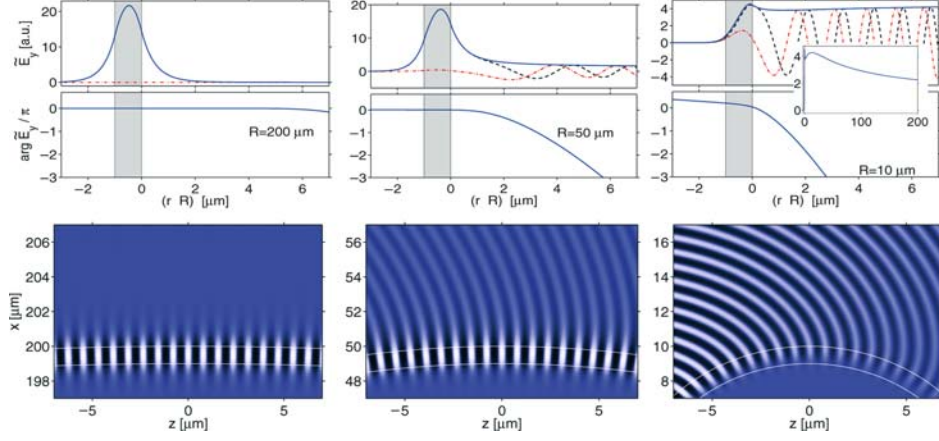


Fig. 4. TE_0 mode profiles for bends according to the setting of Table 1, with different bend radii $R = 200, 50, 10 \mu\text{m}$. First row: radial dependence of the absolute value (solid line), the real and imaginary part (dashed and dash-dotted lines), and the phase of the basic electric field component \tilde{E}_y . The profiles are normalized according to Equation (12), with the global phase adjusted such that $\tilde{E}_y(R)$ is real and positive. Second row: snapshots of the propagating bend modes according to Equation (1). The gray scales correspond to the levels of the real, physical field E_y .

Here β_s is the propagation constant corresponding to the straight waveguide with the width $d = 2w$ and refractive index profile (n_s, n_f, n_s) of the bent waveguide under investigation. Derived quantities are $g^2 = \beta_s^2 - n_s^2 k^2$ and $h^2 = (n_f^2 - n_s^2)k^2 - g^2$. Figure 3 reveals a very good agreement with the attenuation constants calculated by our procedures for bends with low curvature.

3.2. MODE PROFILES

Beyond the values of the propagation constants, the present analytical mode solver permits to evaluate modal fields for the full range of radial coordinates. Figure 4 illustrates normalized profiles for a few fundamental TE bend modes of the configurations considered in Table 1.

One observes the expected effects (Marcuse 1972; Vassallo 1991): Bends with large radii R support modes with almost the familiar symmetric, well confined plane profiles of straight symmetric slab waveguides. With decreasing bend radius, the phase profiles of the bend modes become more and more curved. Along with the increasing attenuation, the maximum of the absolute value of the basic electric field shifts towards the outer rim of the bend, and the relative field levels in the exterior region grow. The mode profiles are essentially complex, with oscillatory behaviour of the real- and imaginary parts of the field profiles in the exterior region. The effects of ‘bending’ and the lossy nature of the bend modes are illustrated best by the snapshots of the physical fields in the second row of Fig. 4.

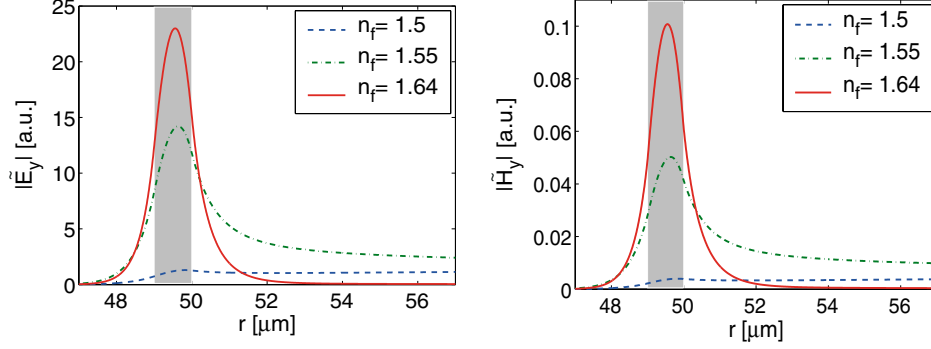


Fig. 5. Fundamental TE (left) and TM mode profiles (right) for symmetric bent slabs with $R = 50 \mu\text{m}$, $\lambda = 1.55 \mu\text{m}$, $d = 1 \mu\text{m}$, $n_s = n_c = 1.45$, and different core refractive indices. As n_f is changed from 1.5 to 1.55 to 1.64, the effective propagation constants γ/k change from $1.4580 - i9.2077 \times 10^{-3}$ to $1.4893 - i1.1624 \times 10^{-3}$ to $1.5598 - i2.1364 \times 10^{-7}$ (TE_0), and from $1.4573 - i1.0088 \times 10^{-2}$ to $1.4862 - i1.6013 \times 10^{-3}$ to $1.5504 - i9.4104 \times 10^{-7}$ (TM_0), respectively.

Just as for straight waveguides, the confinement of the bend modes depends critically upon the refractive index contrast. As exemplified by Fig. 5, one observes quite similar effects when the core refractive index of the bend is varied, as found for the change in bend radius: With loosened confinement and growing attenuation for decreasing n_f , the mode profile maximum shifts towards the outer rim, and the relative field levels in the exterior region increase. Note that all (normalizable) mode profiles decay for large radial coordinates according to Equations (6) and (17), despite their appearance in Figs. 4 and 5 (see the insets in Figs. 4, 7, 9).]

3.3. COMPARISON WITH FDTD RESULTS

As an attempt for a further validation of our results on bend modes we have considered the following numerical experiment. Embedded in a common background, the core of a straight slab waveguide is placed in the vicinity of a ring shaped core of the same width. If a guided wave is launched into the straight channel, by evanescent coupling it excites optical waves that travel around the ring. If, for given polarization, the bent ring waveguide supports only a single low-loss bend mode, one can expect that a field with the corresponding profile establishes itself after a suitable propagation distance. The experiment is carried out in the time domain, with a ramped-up, subsequently time-harmonic excitation, that is advanced over a limited time interval, such that resonance effects can be excluded. Allowing the ‘wave front’ to propagate once around the ring, a

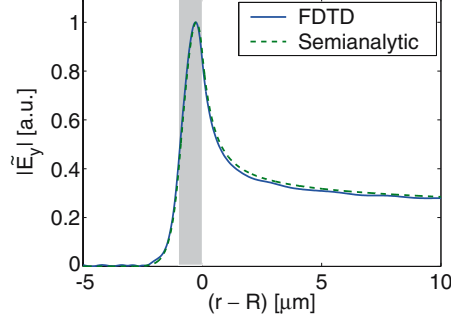


Fig. 6. Bend mode profiles as determined by a FDTD simulation (continuous line) and by the analytical model (dashed curve), for a configuration with $(n_s, n_f, n_c) = (1.6, 1.7, 1.6)$, $d = 1 \mu\text{m}$, $R = 25 \mu\text{m}$, $\lambda = 1.3 \mu\text{m}$. Here the mode profiles are normalized to a unit maximum.

radial field cross section e.g. at an angular position of 90° after the incoupling region can be expected to give an approximation to the bend mode profile. By observing the exponential decay of the ‘stationary’ field for an angular segment after that region, one can estimate the attenuation of the bend mode.

We have applied a standard Finite Difference Time Domain (FDTD) scheme (Yee 1966; Stoffer *et al.* 2000), where a computational window of $80 \times 58 \mu\text{m}^2$ is discretized uniformly by a mesh with step sizes of $0.05 \mu\text{m}$. Perfectly matched layer (PML) boundary conditions enclose the computational domain, with a width of 8 points, a quadratic envelope, and a strength such that the theoretical reflectivity of a wave propagating through the background material at normal incidence is 10^{-6} . The interior of the computational window contains the ring with parameters as given for Fig. 6 and the straight waveguide with the same refractive index profile, with a gap of $0.5 \mu\text{m}$ in between. A modal field is launched into the straight core using the total field/scattered field approach (Taflov 1995). Its amplitude is raised according to a half-Gaussian curve with a waist of 5 fs, with the maximum being reached at 40 fs. After this time, the incident field amplitude is kept constant. The simulation runs for a time of 1.1 ps with a time step of 0.1 fs, after which the ramp of the wave has gone around the ring approximately once.

Figure 6 shows an excellent agreement of the approximation for the bend mode profile obtained in this way with the result of the analytical bend mode solver. We also found a very good agreement of the attenuation constant $\alpha = 0.01949 \mu\text{m}^{-1}$ estimated by the FDTD simulation with the analytic result $\alpha = 0.01978 \mu\text{m}^{-1}$. Hence comparisons of this kind can confirm the expectation that the bend modes as introduced in Equation (1)

Table 3. Propagation constants $\gamma = \beta - i\alpha$ of fundamental modes and first order modes for bent waveguides with $(n_s, n_i, n_c) = (1.6, 1.7, 1.55)$, $d = 2 \mu\text{m}$, $\lambda = 1.55 \mu\text{m}$, for different bend radii R . The value $R = \infty$ indicates the corresponding (bimodal) straight waveguide

$R (\mu\text{m})$	TE ₀			TE ₁			TM ₀			TM ₁		
	β/k	α/k		β/k	α/k		β/k	α/k		β/k	α/k	
∞	1.6775	—		1.6164	—		1.6758	—		1.6134	—	
150	1.6663	≈ 0		1.6037	1.2117×10^{-7}		1.6645	≈ 0		1.6004	3.5259×10^{-7}	
100	1.6611	1.0984×10^{-12}		1.5979	1.7606×10^{-5}		1.6593	1.8446×10^{-12}		1.5946	3.4692×10^{-5}	
50	1.6473	9.6704×10^{-7}		1.5818	1.5113×10^{-3}		1.6451	1.2668×10^{-7}		1.5791	2.0368×10^{-3}	
20	1.6185	1.8299×10^{-3}		1.5283	1.4205×10^{-2}		1.6156	2.1391×10^{-3}		1.5273	1.7868×10^{-2}	
10	1.5890	1.6025×10^{-2}		1.4381	3.4287×10^{-2}		1.5855	1.8702×10^{-2}		1.4391	4.6089×10^{-2}	

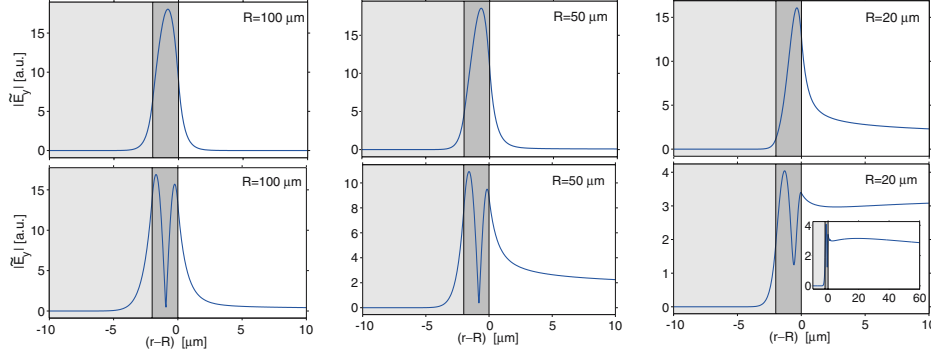


Fig. 7. Fundamental and first order TE modes for the bends of Table 3, absolute values of the basic profile component \tilde{E}_y of structures with radii $R = 100, 50$, and $20 \mu\text{m}$.

are indeed suitable basis fields for a (2D) description of cylindrical microresonator configurations.

3.4. HIGHER ORDER BEND MODES

For cylindrical cavities with relatively high radial refractive index contrast, also higher order bend modes can be relevant for an adequate representation of resonant field patterns (Klunder *et al.* 2000, 2002; Balistreri *et al.* 2001). Table 3 summarizes results for propagation constants of fundamental and first-order modes of both polarizations for a nonsymmetric slab with

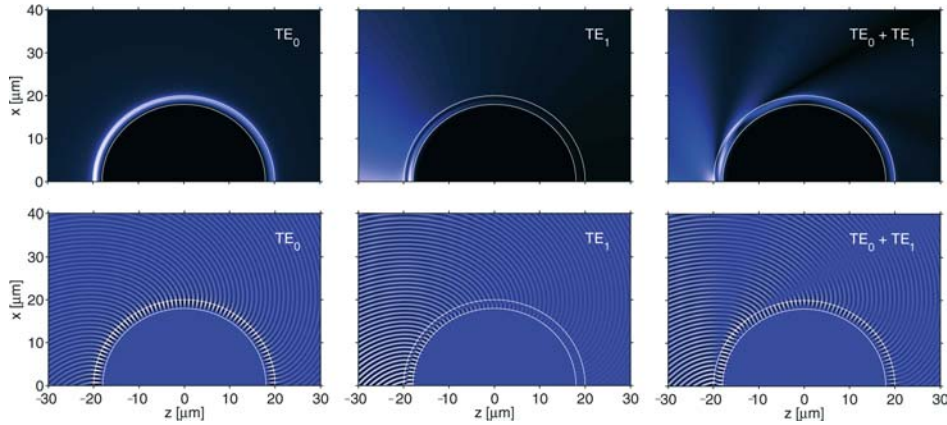


Fig. 8. Spatial evolution and interference of the fundamental and first-order TE modes, for a configuration of Table 3 with $R = 20 \mu\text{m}$. The propagation of the TE_0 mode (left), of the TE_1 mode (center), and of a superposition of these (right) is evaluated. The plots show the absolute value $|E_y|$ (top) and snapshots of the time harmonic physical field E_y (bottom).

decreasing bend radius. In corresponding straight waveguide configuration, the refractive index profile supports two guided modes per polarization orientation.

Just as for the fundamental modes the attenuation of the first order modes grows with decreasing bend radius. Fig. 7 shows that the significantly higher loss levels of the first order modes are accompanied by larger field amplitudes in the exterior region and by a wider radial extent of the mode profiles.

Fig. 8 illustrates the spatial evolution of the TE_0 and TE_1 modes for a configuration with $R = 20 \mu\text{m}$. Major differences between the plots for the single fundamental and first-order fields are the faster decay of the TE_1 mode and the minimum in the radial distribution of that field. The last column of Fig. 8 gives an example for an interference pattern that is generated by a superposition of both modes. Normalized profiles with unit amplitudes and real, positive $\tilde{E}_y(R)$ are initialized at $\theta = 0$, or $z = 0$, respectively (cf. Fig. 1). In the core region one observes the familiar beating process, here in the angular direction, with intensity maxima shifting periodically between the center and the outer rim of the ring. In the exterior region, the mode interference results in a ray-like pattern, where rapidly diverging bundles of waves propagate in directions tangential to the ring, originating from regions around the intensity maxima at the outer ring interface. These phenomena are obscured by the fast decay of the first order mode.

Apart from the fundamental and first-order fields, further higher order modes can be found for the bent slabs of Table 3. While the TE_0 and TE_1 modes considered so far can be viewed as being related to the guided modes supported by a straight slab with the same refractive index profile and thickness, the profiles shown in Fig. 9 are not related to guided modes of that straight waveguide. The classification by the number of minima in the absolute value of the mode profile can still be applied; also the systematics of larger attenuation and higher exterior field levels for growing mode order remains valid.

In contrast to the two lowest order fields, these higher order modes exhibit pronounced intensity maxima in the interior region. Apparently, for the

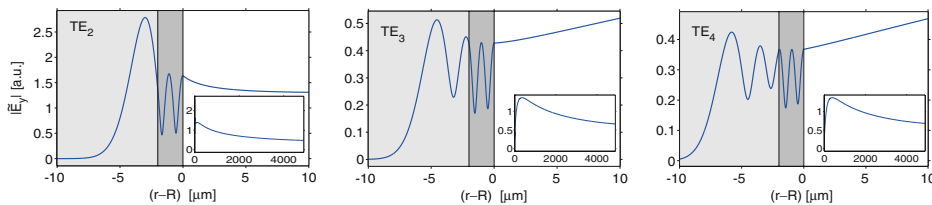


Fig. 9. Higher order TE modes for a bend as considered for Table 3 with $R = 100 \mu\text{m}$. The corresponding propagation constants γ/k are $1.5347 - i2.8974 \times 10^{-3}$ (TE_2), $1.5094 - i5.7969 \times 10^{-3}$ (TE_3), and $1.4891 - i6.1955 \times 10^{-3}$ (TE_4), respectively. The insets clearly show the decay of the mode profiles for $r \rightarrow \infty$ after an initial growth of the field in the cover region.

Table 4. Propagation constants γ for the whispering gallery modes of a curved dielectric interface with the parameters $n_f = 1.5$, $n_c = 1.0$, $R = 4.0 \mu\text{m}$, and $\lambda = 1.0 \mu\text{m}$

	γ/k , present	γ/k , (Stoffer 2001)
TE ₀	$1.3106 - i 1.1294 \times 10^{-5}$	$1.310 - i 1.133 \times 10^{-5}$
TE ₁	$1.1348 - i 1.8862 \times 10^{-3}$	$1.134 - i 1.888 \times 10^{-3}$
TE ₂	$0.9902 - i 1.1676 \times 10^{-2}$	—
TE ₃	$0.8558 - i 1.8832 \times 10^{-2}$	—

present nonsymmetric bend, this indicates the transition to the regime of whispering gallery modes, which is discussed below.

3.5. WHISPERING GALLERY MODES

In contrast to the case of straight waveguide configurations, localized optical waves can propagate along a single curved dielectric interface. The model of Section 2 covers those configurations with the formal choice $n_s = n_f$ in Fig. 1, where d becomes irrelevant. A corresponding ansatz for the mode profile analogous to (6) with merely two pieces leads to a dispersion equation that is considerably simpler than Equation (7). Table 4 and Fig. 10 summarize results for propagation constants and profiles of these whispering gallery modes.

For this example we adopted a set of parameters from Stoffer (2001), that specifies a high-contrast curved interface with a rather small radius, that is, a parameter regime that differs considerably from the previous bent slabs. Still, for growing mode order, qualitatively one finds the increase of the attenuation, the outwards shift of the outermost profile intensity maxima, the raise of the exterior field levels, and the wider radial extent of the profiles, just as for the modes of the bent cores in Figs. 7 and 9. In contrast to the impression

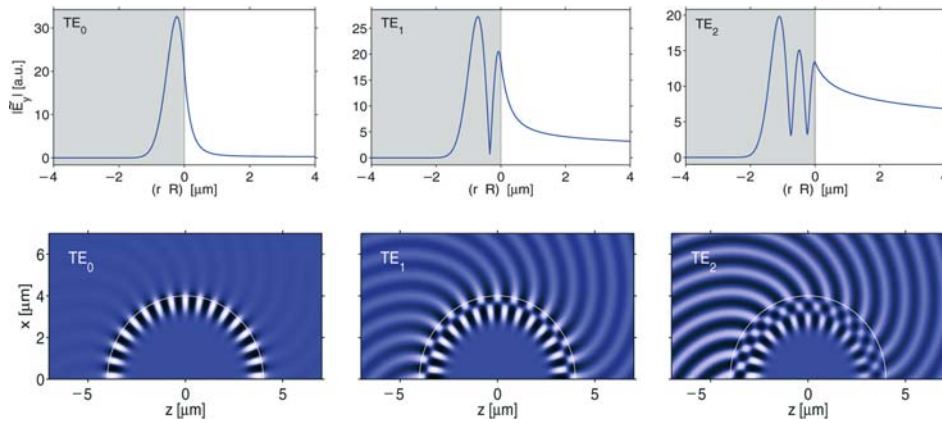


Fig. 10. Profiles (top) and physical field evolution (bottom) of the three lowest order whispering gallery modes according to the specification of Table 4.

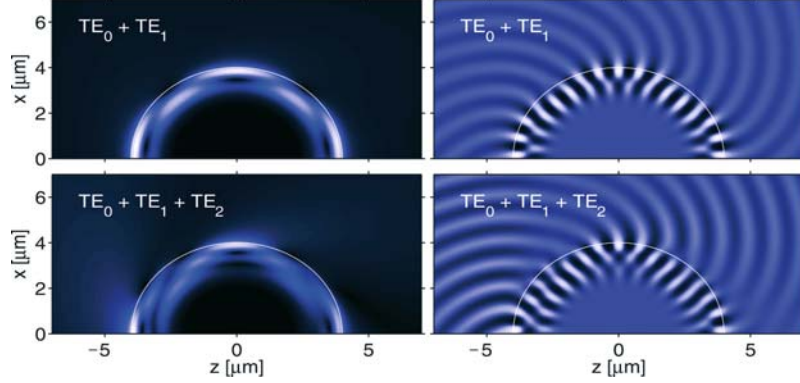


Fig. 11. Interference patterns of the modes of Fig. 10 and Table 4; the plots show the absolute value $|E_y|$ (left) and snapshots of the time harmonic physical field E_y (right). Superpositions of the two (top) and three (bottom) lowest order fields are considered, initialized with unit amplitudes of the normalized profiles (with positive $\tilde{E}_y(R)$) at $z = 0$.

given, for example, in Klunder *et al.* (2000, 2002), the complex mode profiles exhibit minima in the absolute value of the principal field component, not nodal points.

Despite the substantial differences in the attenuation levels of these modes, the higher order fields may well play a role for the representation of resonances of the corresponding disc-shaped microresonator cavity, due to the rather short circumference. Therefore we conclude this paper with two examples of interferences of whispering gallery modes in Fig. 11. As for the bend slabs in Fig. 8 one observes an interior beating pattern and ray-like bundles of waves in the exterior, here on much shorter ranges in terms of the local wavelength.

4. Concluding remarks

In this paper we have reconsidered a classical rigorous analytic model for 2D optical bent slab waveguides and curved dielectric interfaces with piecewise constant refractive index profiles. A frequency domain ansatz in terms of complex order Bessel and Hankel functions leads to an eigenvalue equation (transverse resonance condition) that is to be solved for the complex valued angular mode number.

According to the asymptotic expansions of the relevant Hankel functions, the modal solutions decay as $1/\sqrt{r}$ for growing radial coordinates r , that is specific products of the profile components are integrable along the radial axis. For purposes of bend mode normalization, we could derive quite

compact expressions for the angular modal power. A complex valued inner product of two general fields in the polar coordinate system has been defined, which is suitable to express orthogonality properties of nondegenerate, directional, and polarized modal solutions of the bent waveguide problem.

A series of detailed (benchmark-) examples complements the former abstract reasoning. Concerning propagation constants, these emphasize the arbitrariness in the definition of the bend radius. Examples for profiles of bend modes and for the spatial evolution of the related physical fields are given, for fundamental and higher order modes of bent slabs with relatively small refractive index contrast, as well as for whispering gallery modes supported by high-contrast curved interfaces. A few illustrative examples for interferences of bend modes have been shown, that exhibit a periodic angular beating pattern (apart from the mode decay) in the guiding regions of the bends, and tangential, ray-like bundles of outgoing waves in the exterior regions.

With the present results, a sound analytical basis for (2D) coupled-mode-theory modeling of resonator devices involving microrings or microdisks as cavities has been established. We expect that many of the notions of this paper are directly transferable to the case of 3D configurations involving bent channels with 2D cross sections.

Acknowledgements

Financial support by the European Commission (project IST-2000-28018, 'NAIS') is gratefully acknowledged. The authors thank E. van Groesen, H.J. W.M. Hoekstra, and the colleagues in the NAIS project for many fruitful discussions on the subject.

References

- Abramowitz, M. and I.A. Stegun. *Handbook of Mathematical Functions* (Applied Mathematics Series 55). National Bureau of Standards, Washington, D.C. 1964.
- Amos, D.E. A Portable Package for Bessel Functions of a Complex Argument and Nonnegative Order. <http://www.netlib.org/amos/>, 1983.
- Balistreri, M.L.M., D.J.W. Klunder, F.C. Blom, A. Driessen, J.P. Korterik, L. Kuipers and N.F. van Hulst. *J. Opt. Soc. Am. B* **18** 465, 2001.
- Benech, P., D.A.M. Khalil and F.S. Andr  o. *Opt. Commun.* **88**, 96. 1992.
- Berglund, W. and A. Gopinath. *IEEE J. Lightwave Technol.* **18**, 1161–1166.
- Bertolotti, M., A. Driessen, and F. Michelotti (eds), *Microresonators as Building Blocks for VLSI Photonics*, Vol. 709 of AIP Conference Proceedings. American Institute of Physics, Melville, New York, 2004.
- Bienstman, P., E. Six, A. Roelens, M. Vanwolleghem and R. Baets. *IEEE Photon. Technol. Lett.* **14** 164, 2002.

- Hall, D.G. and B.J. Thompson (eds). *Selected Papers on Coupled-Mode Theory in Guided-Wave Optics*, Vol. MS 84 of *SPIE Milestone Series*. SPIE Optical Engineering Press. Bellingham, Washington USA, 1993.
- Hammer, M., K.R. Hiremath and R. Stoffer. In: *Microresonators as building blocks for VLSI photonics* eds. M. Bertolotti, A. Driessen and F. Michelotti, Vol. 709 of AIP conference proceedings. Melville, New York: American Institute of Physics, pp. 48–71. 2004. Proceedings of the International School of Quantum Electronics, 39th course, Erice, Sicily (October 2003).
- Heiblum, M. and J.H. Harris. *IEEE J. Quantum Electron.* **11** 75, 1975.
- Hiremath, K.R. 'Modeling of 2D Cylindrical Integrated Optical Microresonators'. Master's thesis, University of Twente, Enschede, The Netherlands, 2003.
- Kim, S. and A. Gopinath. *IEEE J. Lightwave Technol.* **14** 2085, 1996.
- Klunder, D., M. Balisteri, F. Blom, J. Hoekstra, A. Driessen, L. Kuipers and N. Van Hulst. *IEEE Photon. Technol. Lett.* **12** 1531, 2001.
- Klunder, D.J.W., M.L.M. Balistreri, F.C. Blom, H.W. J.M. Hoekstra, A. Driessen, L. Kuipers and N.F. van Hulst. *IEEE J. Lightwave Technol.* **20** 519, 2001.
- Klunder, D.J.W., E. Krioukov, F.S. Tan, T. vander Veen, H.F. Bulthuis, G. Sengo, C. Otto, H.W. J.M. Hoekstra and A. Driessen. *Appl. Phys. B* **73**, 603, 2001.
- Lewin, L., D.C. Chang and E.F. Kuester. *Electromagnetic Waves and Curved Structures*. Peter Peregrinus Ltd. (On behalf of IEE), Stevenage, England, 2001.
- Little, B.E., S.T. Chu, H.A. Haus, J. Foresi and J.-P. Laine. *J. Lightwave Technol.* **15** 998, 1997.
- Luke, Y.L. *Integrals of Bessel functions*. McGraw-Hill, New York, 1962.
- Marcatili, E.A.J. *Bell Sys. Tech. J.* **September** 2103, 1969.
- Marcuse, D. *Bell Sys. Tech. J.* **October** 2551, 1971.
- Marcuse, D. *Light Transmission Optics*. Van Nostrand Reinhold Company, New York, USA, 1972.
- Melloni, A., F. Carniel, R. Costa and M. Martinelli. *IEEE J. Lightwave Technol.* **19** 571, 2001.
- Morita, N. and R. Yamada. *IEEE J. Lightwave Technol.* **8** 16, 2001.
- NAIS: project start: 2001, 'Next-generation active integrated optic subsystems'. Information society technologies programme of the European Commission, project IST-2000-28018, <http://www.mesa-plus.utwente.nl/nais/>, 2001.
- Pennings, E.C.M. Bends in Optical Ridge Waveguides, Modelling and Experiment. Ph.D. thesis, Delft University, The Netherlands, 1990.
- Pregla, R. *IEEE J. Lightwave Technol.* **14** 634, 1996.
- Prkna, L.: 'Rotationally symmetric resonant devices in integrated optics'. Ph.D. thesis, Faculty of Mathematics and Physics, Charles University, Prague, Czech Republic, 2004.
- Prkna, L., M. Hubálek and J. Čtyroký. *IEEE Photon. Technol. Lett.* **16** 2057, 2004a.
- Prkna, L., J. Čtyroký and M. Hubálek. *Opt. Quant. Electron.* **36** 259, 2004b.
- Rivera, M. *IEEE J. Lightwave Technol.* **13**, 233, 1995.
- Rowland, D.R. and J.D. Love. *IEE Proceedings, Pt. J* **140** 177, 1993.
- Stoffer, R. 'Uni- and Omnidirectional Simulation Tools for Integrated Optics'. Ph.D. thesis, University of Twente, Enschede, The Netherlands, 2001.
- Stoffer, R., K.R. Hiremath and M. Hammer. In: *Microresonators as building blocks for VLSI photonics*, M. Bertolotti, A. Driessen, and F. Michelotti (eds.): Vol. 709 of AIP conference proceedings. Melville, New York: American Institute of Physics, pp. 366, 2004. Proceedings of the International School of Quantum Electronics, 39th course, Erice, Sicily (October 2003).
- Stoffer, R., H.J.W.M. Hoekstra, R.M. de Ridder, E. van Groesen and F.P.H. van Beckum. *Opt. Quantum Electron.* **32** 94, 2000.
- Taflov, A. *Computational Electrodynamics: The Finite Difference Time Domain Method*. Artech House Inc. Norwood, MA, USA. 1995.
- Temme, N.M. 'Numerical Algorithms for Uniform Airy-type Asymptotic Expansions'. Technical Report MAS-R9706, Centrum voor Wiskunde en Informatica, Amsterdam, The Netherlands, 1997.
- vander Keur, J.M. Propagation Properties of a Circularly Curved, Transversely Inhomogeneous, Dielectric Slab Waveguide'. Technical Report Et/EM 1992–02, Electromagnetic Research Laboratory, Faculty of Electrical Engineering, University of Delft, The Netherlands, 1992.
- Vassallo, C. *Optical Waveguide Concepts*. Elsevier, Amsterdam. 1991.

- Čtyroký, J., L. Prkna, and M. Hubálek: In: *Microresonators as building blocks for VLSI photonics*, M. Bertolotti, A. Driessen, and F. Michelotti eds. Vol. 709 of AIP conference proceedings. Melville, New York: American Institute of Physics, pp. 72–90, 2004. Proceedings of the International School of Quantum Electronics, 39th course, Erice, Sicily (October 2003).
- Wassmann, F. *IEEE Journal of Lightwave Technology* **17**(5), 957, 1999.
- Yamamoto, T. and M. Koshiba. *IEEE J. Lightwave Technol.* **12** 59, 1994.
- Yee, K.S. *IEEE Trans on Antennas and Propagation* **14** 302, 1966.